

Role of the electron spin in determining the coherence of the nuclear spins in a quantum dot

Gunter Wüst, Mathieu Munsch, Franziska Maier, Andreas V. Kuhlmann, Arne Ludwig, Andreas D. Wieck, Daniel Loss, Martino Poggio, and Richard J. Warburton

(Dated: May 20, 2016)

EXPERIMENTAL DETAILS

Sample, microwire and resonance fluorescence

The sample consists of low density self-assembled InGaAs/GaAs quantum dots (QDs) grown by molecular beam epitaxy embedded in the intrinsic region of an n-type GaAs Schottky diode. The tunnel barrier is 25 nm of intrinsic GaAs. The sample is the same as used in our previous experiments [1]; in fact, the QD studied is exactly the same one as in the adiabatic passage experiments [1]. The details of the on-chip microwire and the electrical pulsing are likewise provided in Ref. [1]. All the experiments were carried out at 4.2 K; the nuclear magnetic resonance (NMR) experiments at an external magnetic field of $B_z = 6.6$ T (Faraday geometry).

Initialization and read-out of the nuclear spin polarization is performed optically. We use resonant excitation of the neutral exciton X^0 transition detecting the resonance fluorescence with a confocal dark-field microscope [2]. At $B_z = 0$, the ultra-high quality of the sample is revealed by the small measured linewidth of $1.5 \mu\text{eV}$ [1], close to the ideal transform limit of $\sim 0.9 \mu\text{eV}$. At B_z above about 0.5 T, sweeping the laser frequency across the blue Zeeman transition of the X^0 leads to dynamical nuclear polarization (DNP) via the so called “dragging effect” [3, 4]. The result is a characteristic flat-top spectrum. In practice, the detuning is achieved at constant laser frequency by sweeping the voltage applied to the gate, V_g . For the X^0 , the Stark shift amounts to $0.447 \pm 0.002 \mu\text{eV/mV}$. Following initialization and manipulation, the nuclear spin polarization is read-out by sweeping the optical detuning from a large and negative value. The change in “width” of the dragging plateau (RF pulse compared to no RF pulse) represents the NMR signal. This read-out process is explained in detail in Ref. [1].

Gate switching bandwidth

In principle the characteristic time constant for the charge tunable device is given by RC , where R is the resistance of the back contact and C is the capacitance between top gate and back contact; in practice,

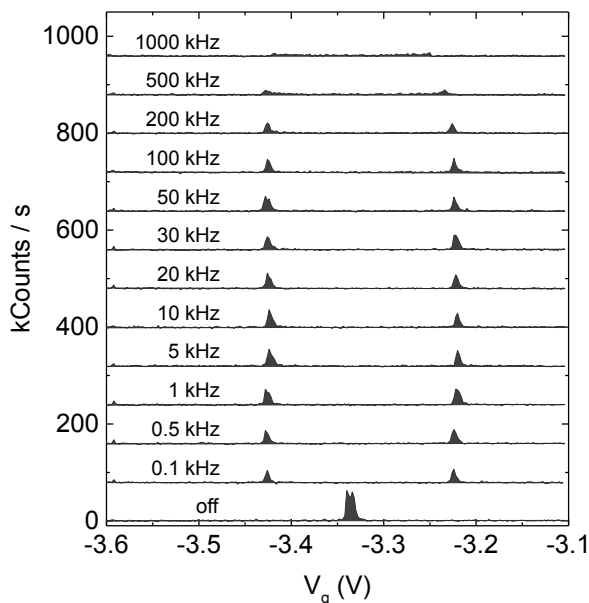


FIG. S1. **Switching speed of the charge tunable device.** Resonance fluorescence spectra of the neutral exciton X^0 on modulating V_g with a square wave ($V_{pp} = 200$ mV) for different frequencies. The maximum bandwidth of the device is ~ 100 kHz.

the device does not behave exactly as an RC -circuit. To measure the bandwidth of the device without making any assumptions on the equivalent circuit, we use the QD itself as a sensor. The gate voltage V_g is modulated with a square wave ($V_{pp} = 200$ mV) and the resonant excitation frequency is fixed. If we now scan the DC component V_g across the X^0 resonance we observe two lines in the resonance fluorescence spectra separated by 200 mV, Fig. S1, provided the modulation frequency is not too high. On increasing the modulation frequency above the bandwidth of the device, the resonance fluorescence peaks become blurred, Fig. S1. In this way we find that the bandwidth of the device is around 100 kHz, i.e. the switching time $\sim 10 \mu\text{s}$. In the experiment, we change the bias following nuclear spin preparation and before nuclear spin manipulation. At the new bias, we introduce a delay of 100 μs before applying the RF pulse. This delay is one order of magnitude larger than the switching time of the device. This delay therefore ensures that the bias at the sample is constant and at the correct value when the RF pulse is applied.

Measurement of the central NMR transition frequency

Since the amplitude and frequency of Rabi oscillations depend sensitively to the RF detuning, it is crucial to determine the resonance frequency of a particular isotope's central frequency with high accuracy.

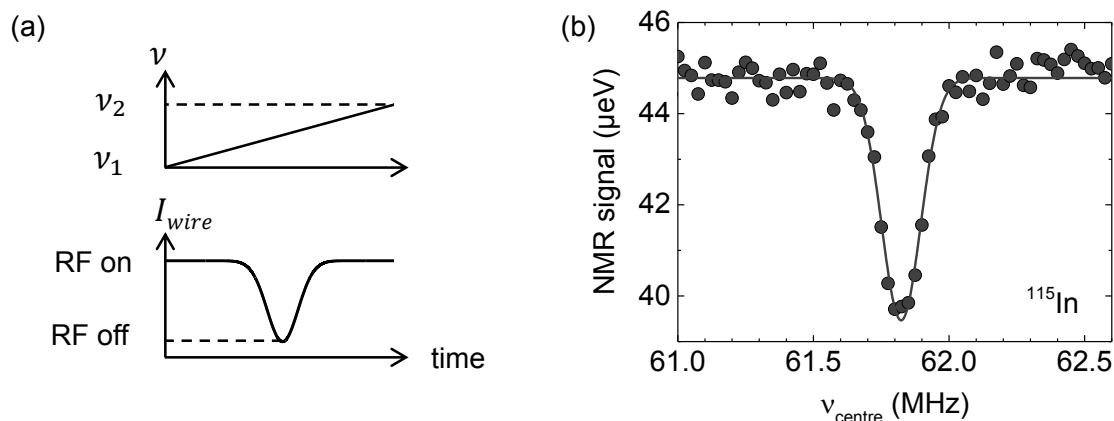


FIG. S2. **Determining the resonance of the central transition.** (a) Sketch of a chirped pulse with a Gaussian amplitude modulation. (b) NMR signal vs centre frequency ν_{centre} of the Gaussian amplitude modulation for indium where $\nu_1 = 49$ MHz, $\nu_2 = 74$ MHz, $\alpha = 10$ GHz/s, FWHM of Gaussian = 0.3 MHz. The solid line is a Gaussian fit. The error on the spectral position is less than 4 kHz.

Our method is to apply a frequency-swept pulse across all the transition frequencies of a particular isotope with a Gaussian amplitude dip where the centre frequency ν_{centre} of the Gaussian can be varied, Fig. S2(a). When ν_{centre} comes close to the central transition, population exchange between the $+\frac{1}{2}$ and $-\frac{1}{2}$ states is interrupted and hence a dip in the NMR signal is observed, Fig. S2(b). From this dip, we determine the central transition frequency with an accuracy of ± 3 kHz for In (± 8 kHz for As), considerably smaller than the Rabi frequency $\nu_{\text{eff}} = 250$ kHz for In ($\nu_{\text{eff}} = 65$ kHz for As) and the 40 kHz linewidth of the In central transition (30 kHz for As) measured at a similar magnetic field [5, 6].

Nuclear spin decay as a function of charging

The DNP decays over time, and this decay time is a strong function of V_g on account of nuclear spin exchange with the Fermi sea in the back contact. To minimize these depolarization effects in the coherent manipulation of the nuclear spins, we keep the total manipulation time short (≤ 50 ms). Even for V_g in between the empty (0) and singly-charged state ($1e$), the so-called “co-tunneling regime”, where the DNP decay rate is fastest, DNP relaxation is negligible for times shorter than 50 ms, Fig. S3. DNP relaxation therefore plays no significant role in the experiment.

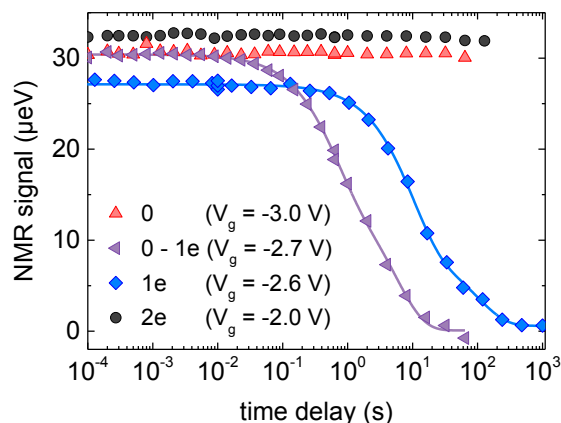


FIG. S3. **Decay of the nuclear spin polarization for different gate voltages.** For an uncharged and a doubly charged QD the nuclear spin polarization decays extremely slowly (order of days). The decay for a singly-charged QD in the region of maximum co-tunneling is much faster, but still slow compared to the time scale of the Hahn echo measurement (50 ms). Solid lines are double exponential fits: $\text{NMR signal} = C_0 + C_1 \exp(-t/\tau_1) + C_2 \exp(-t/\tau_2)$. For $1e$ state close to the plateau centre ($1e$ state with with maximum co-tunneling), the fit yields $C_0 = 12.9 \mu\text{eV}$, $C_1 = 18.0 \mu\text{eV}$, $t_1 = 9.7 \text{ s}$, $C_2 = 8.5 \mu\text{eV}$, $t_2 = 101 \text{ s}$ ($C_0 = 9.6 \mu\text{eV}$, $C_1 = 14.3 \mu\text{eV}$, $t_1 = 0.6 \text{ s}$, $C_2 = 16.0 \mu\text{eV}$, $t_2 = 5.6 \text{ s}$).

g-factors and co-tunneling rate

In the co-tunneling regime in a magnetic field, photoluminescence spectra on the singly-charged exciton X^{1-} show two main peaks with two weak peaks in between. The strong peaks arise from the allowed “vertical” transitions of the X^{1-} , the weak peaks from the “diagonal” transitions. The diagonal transitions are forbidden for ideal selection rules but are weakly allowed in the co-tunneling regime as the co-tunneling interaction weakly hybridizes the electron spin states. The energy separations enable us to determine the electron and hole g-factors, g_e and g_h , respectively. Assuming that $g_e < 0$, for this particular quantum dot, $g_e = -0.67 \pm 0.06$ and $g_h = +1.59 \pm 0.06$. The corresponding gyromagnetic ratios are $\gamma_e = -38.9 \pm 3.4 \mu\text{eV/T}$ and $\gamma_h = 92.3 \pm 3.2 \mu\text{eV/T}$.

We can estimate the co-tunneling rate at the $1e$ plateau edges from the increase in optical linewidth [7]. At both low-bias and high-bias edges, the rate is a few hundred 100 MHz. It is however much more important to determine the co-tunneling rate in the plateau centre. From the standard model of co-tunneling for these structures [8], we can expect that the co-tunneling rate decreases by about 4 orders of magnitude in the plateau centre with respect to the plateau edge. Experimentally, it is challenging to measure sub-MHz rates. However, we estimate the plateau centre co-tunneling rate from the X^{1-} branching ratio (the relative

“forbidden” to “allowed” decay rates), the degree of spin pumping we observe with resonant excitation and from the radiative lifetime. The branching ratio is typically $\sim 0.2\%$ in our sample, a little higher than the values in the literature, 0.05% [9] and 0.08% [10]; the degree of spin pumping is 80% at high magnetic field on the quantum dot in ref. [11]; and the X^{1-} lifetime is ~ 900 ps [11]. This implies a plateau centre co-tunneling rate of ~ 0.2 MHz. There are clearly differences from quantum dot to quantum dot: this analysis establishes an upper limit of 1 MHz on the plateau centre co-tunneling rate.

SIMULATION OF THE RABI OSCILLATIONS

The coherent time evolution for a single spin- $\frac{1}{2}$ system is given by the solutions to the Bloch equations

$$\rho_{11} = \frac{1}{T_1} \rho_{22} + i \frac{\nu_{\text{eff}}}{2} (\rho_{12} - \rho_{21}) \quad (\text{S1})$$

$$\rho_{22} = -\frac{1}{T_1} \rho_{22} + i \frac{\nu_{\text{eff}}}{2} (\rho_{21} - \rho_{12}) \quad (\text{S2})$$

$$\rho_{12} = i \frac{\nu_{\text{eff}}}{2} (\rho_{11} - \rho_{22}) - \left(\frac{1}{T_2} - i\delta\nu \right) \rho_{12} \quad (\text{S3})$$

$$\rho_{21} = i \frac{\nu_{\text{eff}}}{2} (\rho_{22} - \rho_{11}) - \left(\frac{1}{T_2} + i\delta\nu \right) \rho_{21} \quad (\text{S4})$$

where ρ_{ij} are elements of the density matrix, T_1 and T_2 correspond to the relaxation time and decoherence time, ν_{eff} is the effective Rabi coupling and $\delta\nu$ corresponds to the detuning between the RF drive and ν_z . In particular, ρ_{22} gives the population of the upper state and corresponds to the measured data. To account for the spread in centre frequency arising from second order quadrupole shifts, we introduce a Gaussian distribution $\varrho(\delta\nu)$. For a fixed drive frequency, the evolution of the ensemble, $\rho^E(t)$, is given by

$$\rho_{22}^E(t) = \int \varrho(\delta\nu) \rho_{22}(t, \delta\nu) d\delta\nu. \quad (\text{S5})$$

Our procedure starts by fitting the data for the 0 state (the empty quantum dot) taking $T_1 \rightarrow \infty$ and T_2 from the Hahn echo measurement (ms range). From this analysis we derive the width of the frequency distribution as well as the Rabi frequency of the drive. The fit is extremely good. These two parameters are then used as input parameters to describe the $1e$ and $2e$ Rabi oscillations. For the $1e$ and $2e$ states, T_2 is taken from the corresponding Hahn echo experiment.

The procedure works extremely well for ^{115}In ($T_2^{\text{Rabi}} \simeq T_2^{\text{Hahn}}$), see Fig. 2b from the main article. For ^{75}As , a slightly different value for T_2 is required to describe the Rabi oscillations ($T_2^{\text{Rabi}} > T_2^{\text{Hahn}}$), Fig. 2a. We note that an additional broadening of the distribution, arising for instance from the nucleus-dependent Knight field, would amplify the difference.

There is a small difference in the value of the in-plane magnetic field between the experiments on ^{75}As and ^{115}In ($B_{\text{RF}} = 4.4$ mT and 5.2 mT, respectively). This originates from an imperfect description of the

effective strength of the Rabi coupling for high spin number [12]. Indeed, the analytical solutions we use here are only valid in the regime $\nu_Q \gg \nu_{\text{eff}}$, which is, strictly speaking, not true for all spins. That said, the difference between these two values of B_{RF} is small, and the values agree well with the B_{RF} derived in Ref. [1] with a different technique.

THEORETICAL CALCULATION OF DECOHERENCE OF THE NUCLEAR SPIN ENSEMBLE

Decoherence rate of a single nuclear spin

We describe the dynamics of the transverse spin component of a single nuclear spin interacting with a narrowed nuclear spin bath in a quantum dot. The interaction between the nuclei is mediated by a single electron due to hyperfine interactions and we neglect effects due to the dipolar and quadrupole interactions of the nuclear spins. We consider a self-assembled quantum dot loaded with a single electron in a strong magnetic field pointing perpendicular to the substrate, i.e. along z . The Hamiltonian used in this work, $H \simeq H_0 + V$, is only valid in large magnetic fields and corresponds to the effective Hamiltonian derived in Ref. [13] where diagonal terms in V were omitted. The single terms read

$$H_0 = \epsilon_z S_z + \eta_z \sum_j I_j^z + S_z h_z, \quad (\text{S6})$$

$$V = \frac{1}{8\omega} \sum_{j \neq l} A_j A_l \left[\left(\frac{1}{2} + S_z \right) (I_j^- I_l^+ + I_l^- I_j^+) - \left(\frac{1}{2} - S_z \right) (I_j^+ I_l^- + I_l^+ I_j^-) \right]. \quad (\text{S7})$$

Here, S_z is the z component of the electron spin operator, $I_j^{z,\pm}$ ($I_j^\pm = I_j^x \pm iI_j^y$) are the components of the nuclear spin operator of the j th nuclear spin, and ϵ_z and η_z are the electron spin and nuclear spin Zeeman splitting, respectively. The Overhauser field in the z direction is denoted by $h_z = \sum_j A_j I_j^z$ with $A_j = A\nu_0 |\psi(r_j)|^2$, where A is the total hyperfine coupling constant, ν_0 is the volume of a single nucleus unit cell and $\psi(r_j) = \psi(0)e^{-(r_j/a_B)^2/2}$ is the electron envelope function. Here, the effective Bohr radius a_B defines the total number of nuclear spins interacting with the electron spin, N . The effective Zeeman splitting of the electron is given by $\omega \approx \epsilon_z + \langle h_z \rangle = g_e \mu_B B_z + pIA$, where g_e is the electron g factor, μ_B is the Bohr magneton, B_z is the magnetic field along z , p is the nuclear spin polarization and I denotes the nuclear spin. The key assumptions in the theory are that the hyperfine coupling A is smaller than the Zeeman splitting of the electron, $A < \omega$ (perturbation expansion), and that the total nuclear spin decoherence rate is less than the nuclear spin bandwidth $\hat{\Gamma}_N < A/\hbar N$ (Markov approximation).

Following Refs. [13, 14], we describe the transverse nuclear spin dynamics of a single nuclear spin in

the quantum dot. For factorized initial conditions, i.e. $P_k\rho(0) = \rho(0)$, we are able to derive the exact Nakajima-Zwanzig general master equation [15],

$$P_k\dot{\rho}(t) = -iP_kLP_k\rho(t) - i\int_0^t dt'\Sigma(t-t')\rho(t') \quad (\text{S8})$$

with the memory kernel $\Sigma(t) = -iP_kLe^{-iQ_kLt}Q_kLP_k$. Here, we introduced a superoperator P_k that projects onto the subspace of a single nuclear spin k and is defined as $P_k\mathcal{O} = \rho_{eI'}(0)\text{Tr}_{eI'}\mathcal{O}$, with its complement $Q_k = 1 - P_k$. We have $\rho(0) = \rho_e(0) \otimes \rho_I(0)$ and the density matrix $\rho_{eI'} = \rho_e \otimes_{j \neq k} \rho_{i_j}$. Furthermore, $L = L_0 + L_V$ denotes the complete Liouvillian, where $L_0\mathcal{O} = [H_0, \mathcal{O}]$ and $L_V\mathcal{O} = [V, \mathcal{O}]$, respectively. Taking $I = \frac{1}{2}$, we find in the Born approximation,

$$\langle \dot{I}_k^+ \rangle_t = -i\omega_n \langle I_k^+ \rangle_t - i\int_0^t dt'\Sigma_{++}^{(2)}(t-t')\langle I_k^+ \rangle_{t'} \quad (\text{S9})$$

where $\omega_n = \eta_z + A_k[S_z]^{mm} - A_k^2/2\omega$, with $[S_z]^{mm} |m\rangle = S_z |m\rangle$, and where $\Sigma_{++}^{(2)}(t)$ is the matrix element of the memory kernel describing the transverse nuclear spin dynamics to second order in L_V . In Laplace space, the memory kernel is given by

$$\Sigma_{++}^{(2)}(s) = \frac{-i}{16\omega^2} \sum_{j \neq k} \frac{(c_+ + c_-)A_k^2 A_j^2}{s - i[\eta_z + A_j[S_z]^{mm} - A_j^2/2\omega]}, \quad (\text{S10})$$

with the coefficients c_{\pm} defined in Ref. [14]. To remove fast oscillations in Eq. (S9), we transform to a rotating frame with frequency shift $\Delta\omega = -\text{Re}[\Sigma_{++}^{(2)}(s = i(\omega_n + \Delta\omega) + 0^+)]$ determined self-consistently, where 0^+ denotes a positive infinitesimal. In the Born-Markov approximation, the decoherence rate of a single nucleus k is given by $\Gamma_k = -\text{Im}[\Sigma_{++}^{(2)}(s = i(\omega_n + \Delta\omega) + 0^+)]$, see Ref. [16], Appendix C. We find

$$\Gamma_k = \frac{A^3\nu_0^2}{4\pi^5/2\hbar\omega^2 a_B^6} e^{-3(r_k/a_B)^2} \frac{r_k}{a_B}. \quad (\text{S11})$$

In Fig. S4, we plot Γ_k for a realistic set of parameters as a function of r_k . Through energy conservation, the nuclei with the same r_k coordinate interact with each other: this causes the increase in Γ_k at small r_k as the “shells” become progressively larger. At large r_k the interaction becomes weaker and weaker on account of the exponentially decaying electron envelope function.

Decoherence rate of a nuclear spin ensemble

In the NMR experiment, the combined signal of an ensemble of N nuclear spins is measured. We approximate the measured quantity, $\langle I_N^+(t) \rangle$, by

$$\langle I_N^+(t) \rangle \sim \sum_k \langle I_k^+(t) \rangle = \sum_k e^{-\Gamma_k t} \langle I_k^+(0) \rangle \propto \sum_k e^{-\Gamma_k t}, \quad (\text{S12})$$

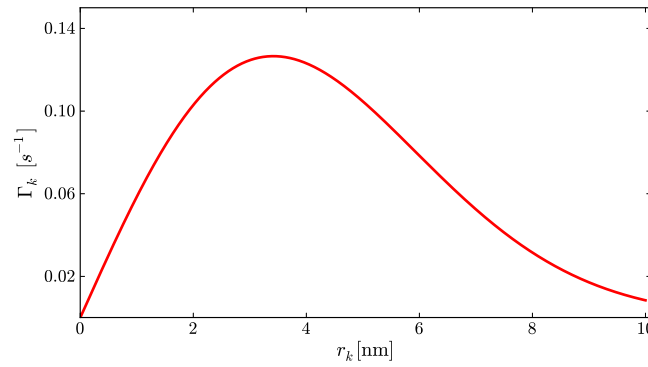


FIG. S4. The decoherence rate Γ_k of a single nuclear spin k as a function of its position r_k in the quantum dot. Here, we assumed an $g = -0.7$, $B = 6$ T, $p = 0.5$, $A = 87 \mu\text{eV}$, $\nu_0 = 23.5 \text{ \AA}^3$ and $N_e = 10^5$, equivalently $a_B = 8.25$ nm.

where the sum \sum_k runs over all nuclear spins contributing to the signal. In the last step, we assumed that $\langle I_k^+(0) \rangle$ is constant over the dot. Note that the brackets describing the averaging, $\langle \dots \rangle$, correspond to different traces for I_N^+ and I_k^+ . For small times t with $\Gamma_k t \ll 1$, we find that

$$\langle I_N^+(t) \rangle \propto N - 1 + e^{-\hat{\Gamma}_N t} \tag{S13}$$

with

$$\hat{\Gamma}_N = \sum_k \Gamma_k = \frac{A^3 \nu_0}{18\pi^{3/2} \hbar \omega^2 a_B^3}. \tag{S14}$$

In Fig. S5, we plot both the exact and approximated decay of $\langle I_N^+(t) \rangle$, again for the parameters given in Fig. S4. We see that approximation captures the onset of the decay quite well. However, at $t \sim 10^{-4}$ s, the approximation starts to deviate from the exact result. Interestingly, the exact result then evolves into a linear decay. The final result for the decoherence rate depends on A^3 . This can be understood as arising from the nuclear spin bandwidth ($\sim A/\hbar N$), where N is a measure of the total number of nuclear spins ($N \propto a_B^3/\nu_0$), multiplied by the electron spin–nuclear spin flip-flop Hamiltonian in second order ($\propto A^2$) [16].

Link of theory to the experiment

The assumptions made in the theory are fulfilled in the experiment: $A \simeq 100 \mu\text{eV}$; $\omega \simeq 250 \mu\text{eV}$ such that $A < \omega$ as required; also, $T_2 \simeq 20 \mu\text{s}$, $\hbar N/A \sim 1 \mu\text{s}$ such that $\hat{\Gamma}_N < A/\hbar N$ as required. The total number of nuclear spins for these quantum dots is known [17]. Specifically, Kloeffel *et al.* replace the

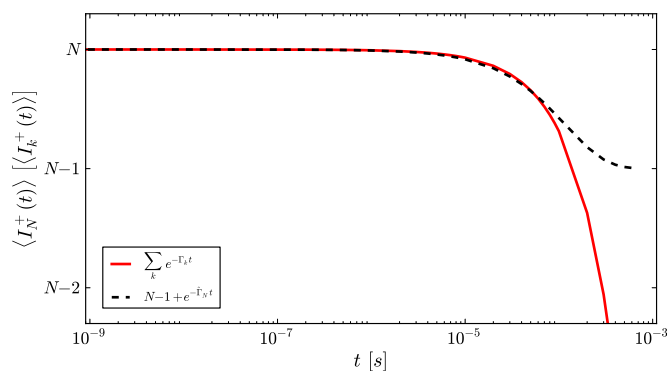


FIG. S5. The NMR signal $\langle I_N^+(t) \rangle$ as a function of t , where we compare the exact (red) and the approximated (black) decay. Here we used the same parameters as given in Fig. S4.

Gaussian envelope function with a top-hat function when defining the number of nuclear spins. Following the same procedure, there are N nuclear spins with

$$\hat{\Gamma}_N = \frac{\sqrt{2}A^3}{9\hbar\omega^2N}. \quad (\text{S15})$$

where $N = 8.5 \times 10^4$ for these quantum dots. (We mention that the simulations in Kloeffel *et al.* are sensitive to the exact value of N .) Of course, the Kloeffel *et al.* quantum dot is not the same one as used here in the NMR experiments. However, the key parameters (emission wavelength, Stark shift, diamagnetic shift, electron g-factor) are very similar. In particular, the diamagnetic shift of the optical transition, which is sensitive to the lateral extent of the electron and hole wave functions, changes little from quantum dot to quantum dot for quantum dots of this type [18]. It is therefore appropriate to take the same value of N with an error on this parameter of $\sim 10\%$.

The Zeeman energy ω is measured on this particular quantum dot by optical spectroscopy. Under the conditions of the NMR experiment, $\omega = 246 \pm 30 \mu\text{eV}$.

So far, the assumption is that all the nuclear spins are coupled together by the electron-mediated nuclear spin–nuclear spin interaction. However, for ^{75}As at high magnetic field and slow electron spin relaxation (i.e. small co-tunneling rate in these experiments), the electron-mediated interaction couples the ^{75}As nuclei but energy conservation suppresses the coupling to the other isotopes. The theory assumes that there is one nuclear spin in a volume of ν_0 . To describe ^{75}As where every other nuclear spin contributes (every group V atom is ^{75}As), the effective volume per ^{75}As nucleus has to be doubled, resulting in

$$\hat{\Gamma}_{\text{As}} = \frac{2\sqrt{2}A_{\text{As}}^3}{9\hbar\omega^2N}, \quad (\text{S16})$$

where N still refers to the total number of nuclear spins in the quantum dot and A is replaced with A_{As} , the hyperfine constant for ^{75}As in GaAs. It is not possible to determine this hyperfine constant in this experiment as we have no independent measure of the exact nuclear polarization created by the optical technique, a standard state of affairs. We therefore take the established value, $A_{\text{As}} = 86 \mu\text{eV}$, listed along with the In and Ga electron hyperfine constants in Ref. [19]. The As value comes originally from Ref. [20], the analysis there relying on a scaling of the result for InSb [21]. Based on the results in these papers, we estimate that the random error in A_{As} is $10 \mu\text{eV}$ ($\sim 12\%$).

For ^{115}In , the hyperfine constant is larger, $110 \mu\text{eV}$ [22], such that A^3 roughly doubles with respect to ^{75}As . However, the situation is more involved. Although the group III concentration ratio In:Ga is 20:80 [1] such that 10% of the total number of atoms are In, it is an exaggeration to expect a factor of ten increase in the effective nuclear volume: the In atoms are likely to be clustered in the centre of the quantum dot. The nuclear spin coherence time is possibly a means to characterize this clustering; here, the uncertainty in T_2 is too large to make a definitive statement. Also, the experimental signal:noise in the Hahn echo at long delays is insufficient to observe any departure from an exponential decay, a prediction of the theory.

-
- [1] Munsch, M. *et al.* Manipulation of the nuclear spin ensemble in a quantum dot with chirped magnetic resonance pulses. *Nature Nanotechnology* **9**, 671–675 (2014).
 - [2] Kuhlmann, A. V. *et al.* A dark-field microscope for background-free detection of resonance fluorescence from single semiconductor quantum dots operating in a set-and-forget mode. *Rev. Sci. Instr.* **84**, 073905 (2013).
 - [3] Latta, C. *et al.* Confluence of resonant laser excitation and bidirectional quantum-dot nuclear-spin polarization. *Nature Physics* **5**, 758–763 (2009).
 - [4] Högele, A. *et al.* Dynamic nuclear spin polarization in the resonant laser excitation of an InGaAs quantum dot. *Phys. Rev. Lett.* **108**, 197403 (2012).
 - [5] Chekhovich, E. A. *et al.* Structural analysis of strained quantum dots using nuclear magnetic resonance. *Nature Nanotechnology* **7**, 646–650 (2012).
 - [6] Chekhovich, E. A., Hopkinson, M., Skolnick, M. S. & Tartakovskii, A. I. Suppression of nuclear spin bath fluctuations in self-assembled quantum dots induced by inhomogeneous strain. *Nature Communications* **6**, 6348 (2015).
 - [7] Kuhlmann, A. V. *et al.* Transform-limited single photons from a single quantum dot. *Nature Communications* **6**, 824 (2015).
 - [8] Smith, J. M. *et al.* Voltage control of the spin dynamics of an exciton in a semiconductor quantum dot. *Phys. Rev. Lett.* **94**, 197402 (2005).
 - [9] Dreiser, J. *et al.* Optical investigations of quantum dot spin dynamics as a function of external electric and magnetic fields. *Phys. Rev. B* **77**, 075317 (2008).

- [10] Lu, C.-Y. *et al.* Direct measurement of spin dynamics in InAs/GaAs quantum dots using time-resolved resonance fluorescence. *Phys. Rev. B* **81**, 035332 (2010).
- [11] Kuhlmann, A. V. *et al.* Charge noise and spin noise in a semiconductor quantum device. *Nature Physics* **9**, 570–575 (2013).
- [12] Van Veenendaal, E., Meier, B. & Kentgens, A. Frequency stepped adiabatic passage excitation of half-integer quadrupolar spin systems. *Molecular Physics* **93**, 195–213 (1998).
- [13] Klauser, D., Coish, W. A. & Loss, D. Nuclear spin dynamics and Zeno effect in quantum dots and defect centers. *Phys. Rev. B* **78**, 205301 (2008).
- [14] Coish, W. A. & Loss, D. Hyperfine interaction in a quantum dot: Non-Markovian electron spin dynamics. *Phys. Rev. B* **70**, 195340 (2004).
- [15] Fick, E. & Sauermann, G. *The Quantum Statistics of Dynamic Processes* (Springer-Verlag, Berlin, 1990).
- [16] Coish, W. A., Fischer, J. & Loss, D. Exponential decay in a spin bath. *Phys. Rev. B* **77**, 125329 (2008).
- [17] Kloeffel, C. *et al.* Controlling the interaction of electron and nuclear spins in a tunnel-coupled quantum dot. *Phys. Rev. Lett.* **106**, 046802 (2011).
- [18] Schulhauser, C. *et al.* Magneto-optical properties of charged excitons in quantum dots. *Phys. Rev. B* **66**, 193303 (2002).
- [19] Coish, W. A. & Baugh, J. Nuclear spins in nanostructures. *physica status solidi (b)* **246**, 2203–2215 (2009).
- [20] Paget, D., Lampel, G., Sapoval, B. & Safarov, V. I. Low field electron-nuclear spin coupling in gallium arsenide under optical pumping conditions. *Phys. Rev. B* **15**, 5780–5796 (1977).
- [21] Gueron, M. Density of the conduction electrons at the nuclei in indium antimonide. *Phys. Rev.* **135**, A200–A205 (1964).
- [22] Coish, W. A., Fischer, J. & Loss, D. Free-induction decay and envelope modulations in a narrowed nuclear spin bath. *Phys. Rev. B* **81** (2010).